Macromolecules

Article

Cite This: Macromolecules 2017, 50, 8274-8278

pubs.acs.org/Macromolecules

Vitrification and Density Scaling of Polyurea at Pressures up to 6 GPa

Timothy C. Ransom,*[,†] Muhtar Ahart,[‡] Russell J. Hemley,[§] and C. Michael Roland*[,†]

[†]Chemistry Division, Naval Research Laboratory, Code 6105, Washington, D.C. 20375-53452, United States

[‡]Geophysical Laboratory, Carnegie Institution of Washington, Washington, D.C. 20015, United States

[§]Department of Civil and Environmental Engineering, The George Washington University, Washington, D.C. 20052, United States

ABSTRACT: Elastomeric polyurea is an important polymer for impact mitigation, but viscoelasticity, nonlinearity, pressure-effects, and the onset of the glass transition complicate analyses of experimental measurements. Consequently, development efforts rely on modeling, which in turn requires accurate potential functions. To address this issue, we measured the glass transition, T_g, of polyurea at pressures up to 6 GPa in a diamond anvil cell. In this method, T_g is determined as the lowest temperature at which the pressure is hydrostatic. From the pressure dependence of T_g, in combination with equation of state measurements at pressures up to 1 GPa, the density scaling exponent for the polyurea was obtained. The value 2.39 ± 0.06 is in accord with previous determinations based on lower pressure experiments; thus, density scaling remains valid for density changes as large as 50%. The scaling exponent reflects the steepness of the intermolecular repulsive potential and should serve as a guide to the choice of potential parameters for simulations of the high strain rate, high pressure dynamics of the material.

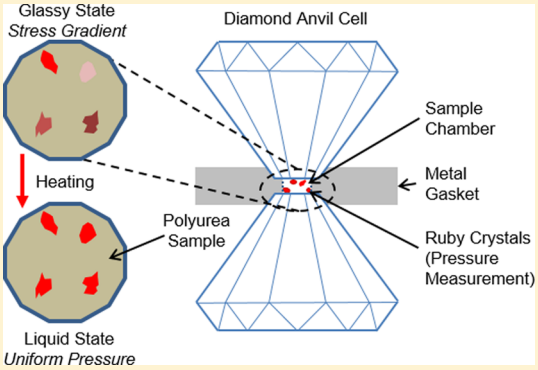

INTRODUCTION

A defining feature of long chain molecules is the marked sensitivity of their dynamics to strain rate. This property can be exploited to obtain large energy dissipation under particular conditions in materials that are otherwise highly elastic.[1] Prominent examples include acoustic dampening,[2] arterial blood flow,[3,4] skid-resistant automobile tires,[5,6] and impact coatings. The last has received a great deal of attention in the past decade in efforts to use polyurea coatings for infrastructure protection and military armor.[7,8] A large amount of experimental data has been acquired to characterize the properties of polyurea under high rates of loading and high pressures.[9−20] However, the impact response of polymers is quite complicated, involving not only viscoelasticity and related thermal effects but also large pressures and material nonlinearities. Because of this complexity, interpretation of experimental data and progress in developing polyurea coatings necessarily require modeling. The models range from phenomenological, wherein the effects of temperature, strain, and pressure are separately measured and then combined empirically,[21−25] to more fundamental treatments that characterize the behavior on the microscopic level.[26−34]

The accuracy of model predictions of dynamic properties depends on the fidelity of the force fields employed. These include contributions from distortion and rupture of covalent bonds and from the nonbonding interactions. Commonly, additivity is assumed, with the potential energy the sum over a van der Waals dispersion term, the Coulombic electrostatic energy, U_{Coulomb}, which for polyurea includes hydrogen bonding, and a term accounting for any changes in the covalent bonds, U_{chain}

$$U = \sum_{i>j}\left[\frac{A_{ij}}{r_{ij}^{\,m}} - \frac{B_{ij}}{r_{ij}^{\,6}}\right] + U_{\text{Coulomb}} + U_{\text{chain}} \tag{1}$$

Here A_{ij} and B_{ij} are constants, r_{ij} is the $i-j$ separation distance, and the sum is over all atoms (or segments in a coarse-grained model). For soft condensed matter, the impact response is governed primarily by the repulsive potential, whereby the value of the exponent m is crucial for reliable computations. The classical value of m = 12 has been assumed in some modeling of polyurea,[28,29] while others have used the COMPASS potential, for which m = 9,[30−33] or a combination of different repulsive exponents.[34]

An experimental means to characterize the steepness of the repulsive potential is from the density scaling relation for the relaxation time τ[35]

$$\tau = f(\rho^{\gamma}/T) \tag{2}$$

in which ρ is the density, T the temperature, f a function, and the scaling variable γ a material constant. From molecular dynamics (MD) simulations it has been shown that the value of γ is determined by the slope of the repulsive potential.[36,37] This is exactly true for a (hypothetical) fluid having an inverse power law repulsive potential

$$U = \left(\frac{A}{r}\right)^{m} \tag{3}$$

Received: August 3, 2017
Revised: September 21, 2017
Published: October 5, 2017

DOI: 10.1021/acs.macromol.7b01676
Macromolecules 2017, 50, 8274−8278

with $m = 3\gamma$.[38,39] It is true to a good approximation for more realistic potentials that include an attractive term.[40,41] However, for molecular liquids the effective slope is somewhat larger than 3γ because the attractive term makes the potential steeper,[37] while for polymers it is found that the slope can be less than 3γ because the intramolecular degrees of freedom (i.e., chain stretching and bending modes) soften the potential.[36] If the density scaling exponent indeed reflects the steepness of the repulsive potential, it follows that different dynamic quantities (τ, viscosity, diffusion constant) should be described by the same value of γ, an expectation that has been verified experimentally.[42]

For unassociated liquids and polymers, the scaling relation has been found to hold over the range of pressures and temperatures accessible by experiment.[35] On the other hand, MD simulations have suggested that deviations from eq 2 occur at very high pressures, manifested as a nonconstant γ.[43] These simulation pressures correspond to density changes in the range 20−30%, substantially larger than for typical experiments (a 1% density changes can alter τ by an order of magnitude[35]). The only putative experimental evidence of a breakdown of the scaling in an unassociated liquid was for decahydroisoquinoline.[43] However, this was subsequently shown to be in error due to an overly long extrapolation of the equation of state (EoS). By measuring the density at pressures up to 1.2 GPa, a more accurate EoS was obtained, and there was no longer any deviations from eq 2.[44] This emphasizes the need for measurements at very high pressures to confirm the generality of the scaling property and inferences drawn from it. This is especially the case for materials such as polyurea used for impact mitigation, for which transient pressures can be extremely high.

Previously we applied eq 2 to relaxation measurements on polyurea that extended to pressures of ∼1 GPa, in combination with an EoS based on data limited to 200 MPa; the obtained $\gamma = 2.35$.[45] This corresponds to $m \sim 7$, smaller than the classical ($m = 12$) and common ($m = 9$) repulsive exponents used in polyurea modeling.[28−34] Herein we describe new results from a novel method[46] employing a diamond anvil cell to extend the pressure range to 6 GPa. In ref 46 high-pressure measurements of T_g showed eq 2 to be valid over very large density ranges for a simple, nonassociated molecular liquid. In the current study, from the pressure dependence of the glass transition we obtain for polyurea $\gamma = 2.39 \pm 0.06$, more accurate but not significantly different from a prior determination.[44] This affirms the validity of density scaling, the application of which often involves extrapolation of measured PVT data. The magnitude of the scaling exponent suggests $m \sim 7$, which is less than the values of m used in recent modeling of polyurea.

EXPERIMENTAL SECTION

Polyurea was prepared by a reaction of Versalink P1000 (Air Products) with Isonate 143 L (Dow Chemical) in a 4:1 mass ratio. Layers 100−200 μm thick were prepared by pressing at ambient temperature, followed by 8 h at 75 °C. The sample was allowed to equilibrate under ambient conditions, with a consequent small water uptake (<1 wt %). A 250 μm diameter disk was cut from the molded sheet and loaded into a diamond anvil cell (DAC). Two diamonds with 700 μm culets formed the top and bottom of the DAC chamber, with a tungsten gasket comprising the sides. The gasket was preindented to 100 μm thickness, with a 250 μm hole drilled in the center to hold the sample. Ruby fluorescence spectroscopy[47] was used for pressure measurements; four ruby chips (5−10 μm diameter) were positioned on the upper culet across the sample prior to closing the chamber. Figure 1 shows the sealed DAC chamber with two rubies, at the center and periphery, indicated (the other two rubies are not easily visible). A 532 nm solid-state laser was used as an excitation source, and fluorescence spectra were collected from each ruby using a Princeton Instruments Acton SP2300 spectrometer equipped with an 1800BLZ grating. The measured doublet spectra were fit with the line shape in ref 48 to yield the pressure, with a relative uncertainty = ±0.05 GPa. An Omega CN380 controlled a band heater wrapped around the DAC for temperature control (±0.5 °C).

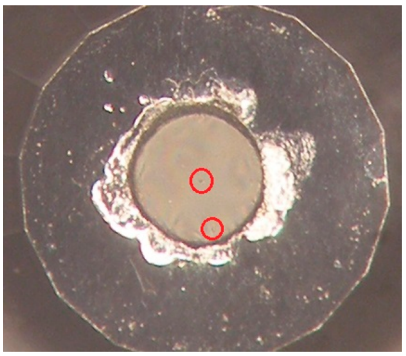

Figure 1. DAC loaded with polyurea and four ruby chips, two of which are circled in red. The irregular, luminous area around the circular sample is the deformed tungsten gasket.

For each measurement of T_g, at ambient temperature the pressure was increased until pressure gradients became evident across the sample, indicating the polyurea had vitrified. Pressure was further increased to a particular initial condition, and the sample was allowed to equilibrate overnight. The DAC and sample were subsequently heated in stepwise fashion, initially in increments of 10−15 K and then in increments of 3 K as T_g was approached. About 15 min was required at each temperature for equilibration, during which the pressured decreased due to thermal expansion of the DAC assembly. Measurement of fluorescence spectra for each of the four rubies was then carried out. The effective rate for these measurements is slow, ∼2×10^{-4} s^{-1}, with physical aging of the glassy sample during the fluorescence measurements introducing a small uncertainty into the data. Heating steps were continued until equivalent fluorescence spectra were obtained from the four rubies, indicating hydrostatic conditions. This defines the glass transition of the sample. The DAC was then cooled to room temperature, and the process repeated with a different initial pressure. The largest density change imposed by the DAC experiment corresponded to a 50% increase at 439 K in going from ambient pressure to 6 GPa. This is the highest temperature used in these experiments, limited by the DAC assembly as well as the increasing overlap at higher temperatures of the ruby fluorescence doublet used to determine the pressure.

In a separate experiment, the volume change of the polyurea was measured as a function of temperature and pressure using a custom bellows and piezometer assembly,[49] loaded into a Manganin cell (Harwood Engineering). Pressure was applied using a manual hydraulic pump and an intensifier (see refs 44 and 45 for details), with Dow Corning 200 silicone oil (viscosity = 50 cst) as the pressurizing medium. The pressure and temperature dependences of the silicone oil volume were determined separately, in order to correct for its contribution to the measured volume changes. The highest pressure achieved in the PVT measurements was about 1 GPa, well below the pressures of the DAC measurements; thus, extrapolation of the EoS was required.

Differential scanning calorimetry (DSC) at atmospheric pressure employed a TA DSC Q100 at heating rates from 0.5 to 10 K/min. The calorimetric glass transition of the polyurea is broad, about 25 K. From the inflection point in the heat capacity curve, $T_g = 208 \pm 2$ K, with values for the different heating rates differing by less than 0.4 K.

DOI: 10.1021/acs.macromol.7b01676
Macromolecules 2017, 50, 8274−8278

RESULTS

Figure 2 shows representative data for the pressure as a function of position within the sample. In the glassy state the pressure is nonuniform, although the stress variations are not systematic with position. These nonuniformities diminish on heating, and at a sufficiently high temperature the fluorescence from each ruby is the same (Figure 2 inset). The temperature for this onset of hydrostatic conditions is taken as T_g. The glass transitions determined in this manner for each pressure are displayed in Figure 3. The data are consistent with the calorimetric T_g measured at a slow heating rate at atmospheric pressure and are parallel to the temperatures for which the dielectric relaxation time equals 0.1 s (the longest τ reported in ref 45). The $T_g(P)$ were fit using the empirical Andersson–Andersson equation[50]

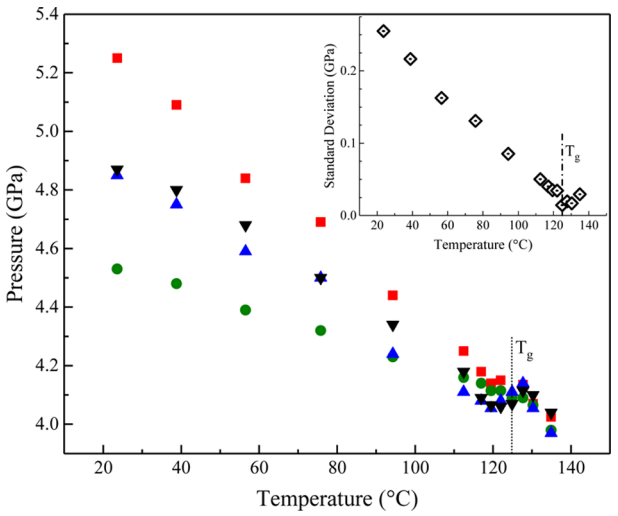

Figure 2. Representative data for the pressure measured from each ruby at temperatures through T_g. There is no systematic spatial variation of pressure in the nonhydrostatic state. For this experiment the lowest P was from the ruby in the middle in Figure 1 (circles), while an intermediate pressure was measured for the ruby at the periphery (inverted triangle). Uncertainties are less than the symbol size. Inset: standard deviation as a function of temperature for the pressure measurements from the four rubies. This reaches a minimum at T = 125 ± 5 °C and P = 4.09 ± 0.1 GPa, defining the glass transition.

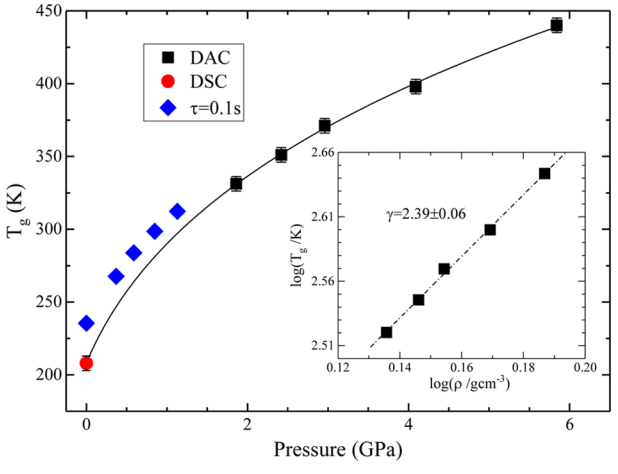

Figure 3. T_g as a function of pressure: DAC (squares); calorimetry (circle); dielectric relaxation time = 0.1 s[45] (diamonds). The line is the fit of eq 4. Inset: double-logarithmic plot of glass transition temperature from the DAC measurements versus density, yielding the scaling exponent γ = 2.39 ± 0.06.

$$T_g = a\left(1 + \frac{b}{c}P\right)^{1/b} \tag{4}$$

yielding a = 208.0 ± 1.9 K, b = 3.55 ± 0.11, and c = 1.58 ± 0.11 GPa; this fit is included in Figure 3. The pressure coefficient at zero pressure, $\left.\frac{dT_g}{dP}\right|_{P=0} = \frac{a}{c}$, equals 132 ± 5 K/GPa, which is at the low end of the range reported for other polymers.[35]

To apply eq 2 requires converting $\tau(T,P)$ to a dependence on T and the specific volume V. To do this, we fit the Tait equation of state[51]

$$V(T,P) = (a_0 + a_1T + a_2T^2) \times \left[1 - C\ln\left(1 + \frac{P}{b_0\exp(-b_1T)}\right)\right] \tag{5}$$

to the PVT measurements, after converting the differential specific volumes to absolute values using the density measured at ambient conditions. The obtained fit parameters for the polyurea, along with the results for the silicone pressurizing fluid, are given in Table 1. The PVT data and fitted Tait equation are shown in Figure 4. Using eq 5 with the parameters in Table 1, the density was calculated for each state point of the DAC experiment; this required extrapolation of the actual PVT measurements. The largest density change in the PVT measurements was about 20% in going from ambient to 1 GPa at 100.7 °C.

The definition of T_g is the temperature below which relaxation times become longer than typical laboratory time scales (e.g., ≥100 s). This means the $T_g(P)$ data in Figure 3 correspond to isochronal conditions. Since τ is constant at T_g, it follows from eq 2 that

$$\log T_g = \gamma \log \rho + \text{const} \tag{6}$$

Thus, a double-logarithmic plot of T_g versus density will be a straight line having a slope equal to the scaling exponent. This analysis was carried out, with the results shown in the inset to Figure 3. The T_g for ambient pressure was omitted from the fit because the DSC and DAC measurements correspond to different τ. The linearity (Pearson correlation coefficient >99%) affirms the applicability of the scaling relation to the polyurea over these large temperature and pressure ranges, and from the slope we obtain γ = 2.39 ± 0.06. This is consistent with the previously reported value, 2.35 ± 0.10, determined from experiments at much lower pressures.[45]

SUMMARY

The main results herein are:

- A novel diamond anvil cell method, based on the deviation from hydrostatic stress in a pressurized glass, was applied for the first time to a polymer.
- Using this method, we determined the pressure coefficient of T_g for polyurea at pressures to 6 GPa (density changes of as much as 50%).
- PVT measurements were obtained up to 1 GPa using a custom belows assembly, greatly increasing the pressure range of the EoS for polyurea.

DOI: 10.1021/acs.macromol.7b01676
Macromolecules 2017, 50, 8274–8278

Table 1. Parameters from Fits of Eq 5

	a_0 (mL/g)	a_1 (mL g^{-1} C^{-1})	a_2 (mL g^{-1} C^{-2})	C	b_0 (GPa)	b_1 (C)
polyurea	0.8999	4.90×10^{-4}	1.75×10^{-7}	0.0889	0.259	3.70×10^{-3}
DC 200 oil	1.0177	1.09×10^{-3}	0	0.0928	0.0882	6.65×10^{-3}

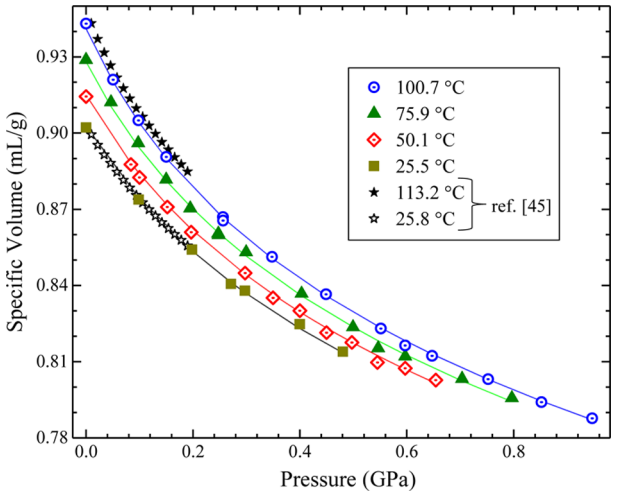

Figure 4. Equation of state data for polyurea, along with the fit to eq 5. Low-pressure measurements from ref 45 (stars) are shown for comparison.

• The data show that the segmental dynamics of polyurea are in accord with the density scaling property expected for nonassociated, amorphous materials. The obtained scaling exponent $\gamma = 2.39 \pm 0.06$, equivalent to a prior determination based on lower pressure data. This underscores the validity of density scaling over very substantial ranges of temperature and density. Molecular modeling of polyurea should employ an intermolecular potential function consistent with this value of γ.

AUTHOR INFORMATION

Corresponding Authors

*E-mail: roland@nrl.navy.mil (C.M.R.).
*E-mail: timothy.ransom.ctr@nrl.navy.mil (T.C.R.).

ORCID

Timothy C. Ransom: 0000-0001-5243-8643
C. Michael Roland: 0000-0001-7619-9202

Notes

The authors declare no competing financial interest.

ACKNOWLEDGMENTS

The work at NRL was supported by the Office of Naval Research, in part by Code 332 (R. G. Barsoum). We thank R. Casalini of NRL and Z. Geballe of the Geophysical Lab for assistance. The facilities used at Carnegie Institution were supported by the US Department of Energy/National Security Administration (DE-NA-0002006, CDAC). T.C.R. acknowledges an American Society for Engineering Education postdoctoral fellowship.

REFERENCES

(1) Roland, C. M. Mechanical behavior of rubber at high strain rates. *Rubber Chem. Technol.* **2006**, *79*, 429−459.
(2) Corsaro, R. D.; Sperling, L. H. *Sound and Vibration Damping with Polymers*; ACS Symposium Series 424; American Chemical Society: Washington, DC, 1990.
(3) Gosline, J. M. Structure and mechanical-properties of rubber-like proteins in animals. *Rubber Chem. Technol.* **1987**, *60*, 417−438.
(4) Lillie, M. A.; Gosline, J. M. The effects of hydration on the dynamic mechanical-properties of elastin. *Biopolymers* **1990**, *29*, 1147−1160.
(5) Heinrich, G.; Dumler, H. B. Wet skid properties of filled rubbers and the rubber—glass transition. *Rubber Chem. Technol.* **1998**, *71*, 53−61.
(6) Takino, H.; Nakayama, R.; Yamada, Y.; Kohjiya, S.; Matsuo, T. Viscoelastic properties of elastomers and tire wet skid resistance. *Rubber Chem. Technol.* **1997**, *70*, 584−594.
(7) Barsoum, R. G. S. *Elastomeric Polymers with High Rate Sensitivity: Applications in Blast, Shockwave, and Penetration Mechanics*; William Andrew: 2015.
(8) Iqbal, N.; Tripathi, M.; Parthasarathy, S.; Kumar, D.; Roy, P. Polyurea coatings for enhanced blast-mitigation: a review. *RSC Adv.* **2016**, *6*, 109706.
(9) Hsieh, A. J.; Chantawansri, T. L.; Hu, W.; Strawhecker, K. E.; Casem, D. T.; Eliason, J. K.; Nelson, K. A.; Parsons, E. M. New insight into microstructure-mediated segmental dynamics in select model poly(urethane urea) elastomers. *Polymer* **2014**, *55*, 1883−1892.
(10) Jiao, T.; Clifton, R. J.; Grunschel, S. E.; Furnish, M. D.; Elert, M.; Russell, T. P.; White, C. T. High Strain Rate Response of an Elastomer in Shock Compression of Condensed Matter − 2005. *Am. Inst. Phys.* **2006**, No. 845, 809−812.
(11) Amini, M.; Isaacs, J.; Nemat-Nasser, S. Experimental Investigation of Response of Monolithic and Bilayer Plates to Impulsive Loads. *Int. J. Impact Eng.* **2010**, *37*, 82−89.
(12) Amini, M.; Nemat-Nasser, S. Micromechanisms of ductile fracturing of DH-36 steel plates under impulsive loads and influence of polyurea reinforcing. *Int. J. Fract.* **2010**, *162*, 205−217.
(13) Xue, L.; Mock, W.; Belytschko, T. Penetration of DH-36 steel plates with and without polyurea coating. *Mech. Mater.* **2010**, *42*, 981−1003.
(14) Chakkarapani, V.; Ravi-Chandar, K.; Liechti, K. Characterization of Multiaxial Constitutive Properties of Rubbery Polymers. *J. Eng. Mater. Technol.* **2006**, *128*, 489−494.
(15) Tekalur, S. A.; Shukla, A.; Shivakumar, K. Blast resistance of polyurea based layered composite materials. *Comp. Struc* **2008**, *84*, 271−281.
(16) Yi, J.; Boyce, M.; Lee, G.; Balizer, E. Large deformation rate-dependent stress−strain behavior of polyurea and polyurethanes. *Polymer* **2006**, *47*, 319−329.
(17) Roland, C.; Twigg, J.; Vu, Y.; Mott, P. High strain rate mechanical behavior of polyurea. *Polymer* **2007**, *48*, 574−578.
(18) Pathak, J.; Twigg, J.; Nugent, K.; Ho, D.; Lin, E.; Mott, P.; Robertson, C.; Vukmir, M.; Epps, T., III; Roland, C. *Macromolecules* **2008**, *41*, 7543−7548.
(19) Choi, T.; Fragiadakis, D.; Roland, C. M.; Runt, J. Microstructure and segmental dynamics of polyurea under uniaxial deformation. *Macromolecules* **2012**, *45*, 3581−3589.
(20) Mott, P.; Giller, C.; Fragiadakis, D.; Rosenberg, D.; Roland, C. Deformation of polyurea: Where does the energy go? *Polymer* **2016**, *105*, 227−233.
(21) Li, C.; Lua, J. A hyper-viscoelastic constitutive model for polyurea. *Mater. Lett.* **2009**, *63*, 877−880.
(22) Mohotti, D.; Ali, M.; Ngo, T.; Lu, J.; Mendis, P. Strain rate dependent constitutive model for predicting the material behaviour of polyurea under high strain rate tensile loading. *Mater. Eng.* **2014**, *53*, 830−837.
(23) El Sayed, T.; Mock, W.; Mota, A.; Fraternali, F.; Ortiz, M. Computational assessment of ballistic impact on a high strength

DOI: 10.1021/acs.macromol.7b01676
Macromolecules 2017, 50, 8274−8278

structural steel/polyurea composite plate. *Comput. Mech.* **2009**, *43*, 525−534.
(24) Xue, Z.; Hutchinson, J. W. Neck development in metal/elastomer bilayers under dynamic stretchings. *Int. J. Solids Struct.* **2008**, *45*, 3769−3778.
(25) Clifton, R. J.; Wang, X.; Jiao, T. A physically-based, quasilinear viscoelasticity model for the dynamic response of polyurea. *J. Mech. Phys. Solids* **2016**, *93*, 8−15.
(26) Grujicic, M.; Pandurangan, B.; He, T.; Cheeseman, B.; Yen, C.-F.; Randow, C. Computational investigation of impact energy absorption capability of polyurea coatings via deformation-induced glass transition. *Mater. Sci. Eng., A* **2010**, *527*, 7741−7751.
(27) Grujicic, M.; Pandurangan, B.; King, A.; Runt, J.; Tarter, J.; Dillon, G. Multi-length scale modeling and analysis of microstructure evolution and mechanical properties in polyurea. *J. Mater. Sci.* **2011**, *46*, 1767−1779.
(28) Cui, Z.; Brinson, L. C. Thermomechanical properties and deformation of coarse-grained models of hard-soft block copolymers. *Phys. Rev. E* **2013**, *88*, 022602.
(29) Arman, B.; Reddy, A. S.; Arya, G. Viscoelastic properties and shock response of coarse-grained models of multiblock versus diblock copolymers: insights into dissipative properties of polyurea. *Macromolecules* **2012**, *45*, 3247−3255.
(30) Agrawal, V.; Holzworth, K.; Nantasetphong, W.; Amirkhizi, A. V.; Oswald, J.; Nemat-Nasser, S. Prediction of Viscoelastic Properties with Coarse-Grained Molecular Dynamics and Experimental Validation for a Benchmark Polyurea System. *J. Polym. Sci., Part B: Polym. Phys.* **2016**, *54*, 797−810.
(31) Grujicic, M.; Yavari, R.; Snipes, J.; Ramaswami, S.; Jiao, T.; Clifton, R. Experimental and Computational Study of the Shearing Resistance of Polyurea at High Pressures and High Strain Rates. *J. Mater. Eng. Perform.* **2015**, *24*, 778−798.
(32) Grujicic, M.; Yavari, R.; Snipes, J.; Ramaswami, S.; Runt, J.; Tarter, J.; Dillon, G. Molecular-level computational investigation of shock-wave mitigation capability of polyurea. *J. Mater. Sci.* **2012**, *47*, 8197−8225.
(33) Agrawal, V.; Arya, G.; Oswald, J. Simultaneous Iterative Boltzmann Inversion for Coarse-Graining of Polyurea. *Macromolecules* **2014**, *47*, 3378−3389.
(34) Grujicic, M.; Snipes, J.; Ramaswami, S.; Yavari, R.; Runt, J.; Tarter, J.; Dillon, G. Coarse-grained molecular-level analysis of polyurea properties and shock-mitigation potential. *J. Mater. Eng. Perform.* **2013**, *22*, 1964−1981.
(35) Roland, C. M.; Hensel-Bielowka, S.; Paluch, M.; Casalini, R. Supercooled dynamics of glass-forming liquids and polymers under hydrostatic pressure. *Rep. Prog. Phys.* **2005**, *68*, 1405−1478.
(36) Roland, C. M.; Bair, S.; Casalini, R. Thermodynamic scaling of the viscosity of van der Waals, H-bonded, and ionic liquids. *J. Chem. Phys.* **2006**, *125*, 124508.
(37) Coslovich, D.; Roland, C. Thermodynamic scaling of diffusion in supercooled Lennard-Jones liquids. *J. Phys. Chem. B* **2008**, *112*, 1329−1332.
(38) Hoover, W.; Rossj, M. Statistical theories of melting. *Contemp. Phys.* **1971**, *12*, 339−356.
(39) March, N. H.; Tosi, M. P. *Introduction to Liquid State Physics*; World Scientific: Singapore, 2002.
(40) Bailey, N. P.; Pedersen, U. R.; Gnan, N.; Schrøder, T. B.; Dyre, J. C. Pressure-energy correlations in liquids. I. Results from computer simulations. *J. Chem. Phys.* **2008**, *129*, 184507.
(41) Bailey, N. P.; Pedersen, U. R.; Gnan, N.; Schrøder, T. B.; Dyre, J. C. Pressure-energy correlations in liquids. II. Analysis and consequences. *J. Chem. Phys.* **2008**, *129*, 184508.
(42) Casalini, R.; Bair, S. S.; Roland, C. M. Density scaling and decoupling in o-terphenyl, salol, and dibutyphthalate. *J. Chem. Phys.* **2016**, *145*, 064502.
(43) Bøhling, L.; Ingebrigtsen, T. S.; Grzybowski, A.; Paluch, M.; Dyre, J. C.; Schrøder, T. B. Scaling of viscous dynamics in simple liquids: theory, simulation and experiment. *New J. Phys.* **2012**, *14*, 113035.
(44) Casalini, R.; Roland, C. M. The "anomalous" dynamics of decahyroisoquinoline revisited. *J. Chem. Phys.* **2016**, *144*, 024502.
(45) Roland, C.; Casalini, R. Effect of hydrostatic pressure on the viscoelastic response of polyurea. *Polymer* **2007**, *48*, 5747−5752.
(46) Ransom, T. C.; Oliver, W. F. Glass transition temperature and density scaling in cumene at very high pressure. *Phys. Rev. Lett.* **2017**, *119*, 025702.
(47) Piermarini, G. J.; Block, S.; Barnett, J. D.; Forman, R. A. Calibration of the pressure dependence of the R 1 ruby fluorescence line to 195 kbar. *J. Appl. Phys.* **1975**, *46*, 2774−2780.
(48) Munro, R. G.; Piermarini, G. J.; Block, S.; Holzapfel, W. B. Model line-shape analysis for the ruby R lines used for pressure measurement. *J. Appl. Phys.* **1985**, *57* (165), 165.
(49) Bair, S. S. *High Pressure Rheology for Quantitative Elastohydrodynamics*; Elsevier: 2007; Vol. *54*.
(50) Andersson, S. P.; Andersson, O. Relaxation studies of poly(propylene glycol) under high pressure. *Macromolecules* **1998**, *31*, 2999−3006.
(51) Zoller, P.; Walsh, D. *Standard Pressure-Volume-Temperature Data for Polymers*; Technomic: Lancaster, PA, 1995.

DOI: 10.1021/acs.macromol.7b01676
Macromolecules 2017, 50, 8274−8278